Histol Histopathol (2023) 38: 623-636

https://www.hh.um.es

Histology and Histopathology
From Cell Biology to Tissue Engineering

ORIGINAL ARTICLE **Open Access**

Earliest histopathological changes in COVID-19 pneumonia with comprehensive gene expression analyses: A case series study

Koji Okudela[1], Hiroyuki Hayashi[2], Yukihiro Yoshimura[3], Hiroaki Sasaki[3], Nobuyuki Miyata[4], Hiromichi Iwashita[1], Toshiaki Kataoka[1], Mai Matsumura[1], Hideaki Mitsui[1], Yasuyoshi Hatayama[5], Tsuneo Yamashiro[6], Akihide Ryo[5] and Natsuo Tachikawa[2]

Departments of [1]Pathology, [5]Microbiology, and [6]Radiology, Yokohama City University Graduate School of Medicine; Division of [2]Pathology, [3]Infectious Disease and [4]Respiratory Medicine, Yokohama Municipal Citizen's Hospital, Yokohama, Japan

Summary. Aims. In COVID-19 pneumonia, early detection and appropriate treatment are essential to prevent severe exacerbation. Therefore, it is important to understand the initiating events of COVID-19 pneumonia. However, at present, the literature about early stage disease has been very limited. Here, we investigated the earliest histopathological changes and gene expression profiles associated with COVID-19 pneumonia.

Methods and Results. We carefully examined 25 autopsied cases with different clinical courses. Dilation of capillaries and edematous thickening of the alveolar septa were found even in areas that macroscopically looked almost normal. Pneumocytes, histocytes/macrophages, and vascular endothelial cells were immunohistochemically positive for tissue factor, which is an important early responder to tissue injuries. Comprehensive gene expression analyses revealed that those lesions presented differential profiles compared to those of control lungs and were associated with a significant upregulation of the lysosomal pathway.

Conclusions. Alveolar capillary dilation and edematous thickening may be the earliest histopathological change detected in COVID-19 pneumonia. Intensive investigations of such lesions may lead to an understanding of the initiating event of not only COVID-19 pneumonia but also of general diffuse alveolar damage.

Key words: COVID-19, Diffuse alveolar damage, Earliest histopathological change

Corresponding Author: Koji Okudela, M.D., Ph.D., Department of Pathology, Yokohama City University Graduate School of Medicine, Yokohama, Japan. e-mail: kojixok@yokohama-cu.ac.jp

DOI: 10.14670/HH-18-557

Introduction

Coronavirus disease 19 (COVID-19) has rapidly spread worldwide since the end of 2019, causing more than 400-million documented cases and 5.7-million deaths to date (February 2022) (https://ourworldindata.org/coronavirus-data). One crucial feature of COVID-19 is its high mortality rate, which is substantially higher than that of the seasonal influenza (~15% versus ~0.1%) (Okudela et al., 2020). Although the newly developed vaccines supplied worldwide are conquering this pandemic, COVID-19 remains detrimental, causing a large number of deaths every day.

Throughout the COVID-19 pandemic, hundreds of autopsy case reports were published in the English literature (Okudela et al., 2020; Borczuk, 2021; Hooper et al., 2021; Maiese et al., 2021). Accumulating evidence has confirmed that the most critical pathological event is pneumonia, spatially and temporally intermittently inducing alveolar damage (Borczuk, 2021). Different pathological changes can be observed even in a single histological section, such as exudative lesions with hyaline membranes and proliferative lesions with pneumocytes, histocytes/macrophages, and myofibroblastic cell proliferation (Bosmuller et al., 2021; Maiese et al., 2021).

Several recent review articles mentioned temporal histological changes by dividing four main morphological stages: early, exudative, proliferative, and fibrotic. Generally, the exudative stage lasts from 3 to 7 days after the onset, followed by the proliferative and fibrotic stages for several weeks (Thompson et al., 2017; Borczuk, 2021; Bosmuller et al., 2021). However, descriptions of the early stage are very limited and are virtually based on incidental findings from a handful of cases including patients undergoing surgery for lung cancer (Pernazza et al., 2020; Tian et al., 2020; Bosmuller et al., 2021). The reports suggest that focal

edema, pneumocyte damage and hyperplasia, macrophage desquamation, and endothelialitis/capillaritis can be observed at this stage (Pernazza et al., 2020; Tian et al., 2020; Bosmuller et al., 2021). Early detection and treatment are necessary to prevent severe exacerbation; thus, it is essential to understand the initiating events.

In this study, we carefully examined a series of COVID-19 autopsy cases, specifically the temporal histopathological changes in alveolar damage, and revealed the earliest histopathological changes.

Materials and methods

Autopsy series

A total of 25 COVID-19 autopsy cases from Yokohama Citizens Municipal hospital were carefully examined histologically. Of them, the 5 cases suitable for this study (shorter clinical cause with early COVID-19 pneumonia) were chosen for morphometrical and gene expression analyses. Baseline information, such as age, gender, CT-severity score (Pan et al., 2020), results of PCR test, and essential autopsy results, of all the 25 COVID-19 cases and 5 control causes are summarized in Table 1. The Ethics Committees of Yokohama City University (approving number, A130926004/B201200074) and Yokohama Citizens' Municipal Hospital (approving number, 20-11-05) approved this study.

Conventional histopathological examination

Lung tissues were fixed by injecting 10% buffered formaldehyde solution through the bronchus and immersed in the solution for around 10 days. Consequently, tissues were paraffin-embedded and stained with hematoxylin and eosin, Elastica van Gieson, and Alcian blue periodic acid Schiff.

RT-PCR analysis

RT-PCR on the secretory fluids (nasal swab, saliva, or sputum) for SARS-CoV2 was performed with LightMix (TIB MOLBIOL, Berlin, Germany). Cycle threshold less than 40 was judged as positive. RT-PCR on the autopsied lung tissues was according to the method described elsewhere (Yamaoka et al., 2021). Copy number more than 10 per μg was judged as positive.

Immunohistochemistry

Tissue sections were incubated with a blocking solution (3% hydrogen peroxide/5% goat serum) to inhibit endogenous peroxidases and non-specific protein binding and were boiled in an antigen retrieval buffer. The sections were then incubated with the primary antibody against CD34 (mouse monoclonal antibody clone QBEND/10.4.19, Immunotech, Marseille, France), SARS-CoV-2 nucleocapsid (mouse monoclonal antibody clone 001, Sino Biological, Beijing, China), tissue factor (TF) (rabbit polyclonal antibody, Santa Cruz, Santa Cruz, CA), cathepsin B (CSTB) (mouse monoclonal antibody clone CA10, Abcam, Cambridge, MA), followed by incubation with a horseradish peroxidase-labeled anti-mouse immunoglobulin antibody. Immunoreactivity was visualized using diaminobenzidine as a substrate, and the nuclei were lightly counterstained with hematoxylin.

Morphometry

Glass slides were scanned using a virtual slide system (NanoZoomer slide scanner, Hamamatsu Photonics, Hamamatsu, Japan). Morphometrical analyses were performed using the freely published software NDP.view2 (Hamamatsu Photonics, Hamamatsu, Japan).

Statistical analysis

The relationships between the diameters of the capillary and alveolar septa and the earliest alveolar damage were analyzed using the Wilcoxon/Kruskal-Wallis test. Statistical analyses were conducted using JMP (version 15.0; SAS Institute Inc., Cary, NC).

Gene-chip microarray analysis

Total RNA was extracted using an RNeasy® Micro Kit (Qiagen, Venlo, Netherlands) and then subjected to comprehensive mRNA expression analyses with Clariome^{TM} D assay (Thermo fisher scientific, Waltham, MA). We here examined 2 COVID-19 autopsied lung tissues and 2 control (autopsied lungs that looked almost normal histologically) for the comprehensive analysis. The Kyoto Encyclopedia of Genes and Genomes (KEGG) pathway analysis was performed using a public software (DAVID, Laboratory of Human Retrovirology and Immunoinformatics, Frederick, MD).

Results

Conventional histological examination

A representative case with a 10-day disease history is shown. Grossly, the cut surface of the lung showed a mosaic appearance. Some areas looked slightly gray-whiteish, while the others looked almost normal. The macroscopic photograph and corresponding CT slice are shown in Fig. 1. Histologically, the slightly gray-white areas were exudative stage of alveolar damage with hyaline membranes (Fig. 2A (square 1), and 2B), and the areas that looked almost normal also showed faint but interesting histological changes, such as capillary dilation and edematous thickening of alveolar septa occasionally with a small number of assembled

Table 1. Essential information of autopsy cases examined in the present study.

Category/ Case	Age (year-old)	Gender	Whole duration (from exacerbation) (days)	CT score (at day after onset) (day	RT-PCR Secretory fluid	Cause of death	Main comorbidity	Postmortem (hour)	RT-PCR Autopsy lung	IHC Autopsy lung	His	Mor	Exp	Sample name
COVID-19														
COV001	93	F	10 (6)	15 (1)	+	DAD / Respiratory failure	Bronchopneumonia severe	12	+	+	*	*	*	E1
COV002	84	M	15 (15)	N/D	+	DAD / Respiratory failure	N/A	47	+	+	*			
COV003	93	F	20 (16)	9 (5)	+	Amyloidosis / Circulation failure	N/A	13	-	-	*			
COV004	85	M	24 (22)	8 (3)	+	DAD / Respiratory failure	Bronchopneumonia severe	66	+	-	*			
COV005	70	M	14 (9)	N/D	+	DAD / Respiratory failure	Idiopathic pulmonary fibrosis	77	+	-	*			
COV006	86	F	12 (6)	25 (12) AI	+	DAD / Respiratory failure	N/A	17	+	+	*	*	*	E2
COV007	86	F	27 (3)	9 (6)	+	DAD / Respiratory failure	Angiosarcoma systemic metastasis	26	+	+	*			
COV008	82	F	19 (12)	N/D	+	DAD / Respiratory failure	Pulmonary artery thrombosis	20	+	-	*			
COV009	74	M	14 (7)	18 (7)	+	DAD / Respiratory failure	Acute monocytic leukemia	20	+	+	*	*		E4
COV010	77	M	25 (17)	23 (9)	+	DAD / Respiratory failure	Bronchopneumonia mild	15	+	-	*			
COV011	88	F	20 (17)	14 (4)	+	DAD / Respiratory failure	Rheumatoid arthritis	25	+	-	*			
COV012	89	F	14 (5)	25 (14) AI	+	DAD / Respiratory failure	N/A	24	+	+	*	*		E5
COV013	77	M	27 (17)	14 (11)	+	DAD / Respiratory failure	AMI / Systemic thrombosis	24	-	-	*			
COV014	73	M	38 (10)	14 (18)	+	DAD / Respiratory failure	AMI / Sepsis	83	+	-	*			
COV015	91	M	27 (24)	18 (4)	+	DAD / Respiratory failure	Sepsis / Prostatic cancer localized	24	+	-	*			
COV016	75	M	41 (35)	20 (7)	+	DAD / Respiratory failure	Sepsis / Lung cancer localized	11	+	-	*			
COV017	91	M	36 (30)	13 (7)	+	DAD / Respiratory failure	Rheumatoid arthritis / Gastric cancer localized	5	+	-	*			
COV018	79	M	86 (79)	17 (8)	+	DAD / Respiratory failure	Bronchopneumonia mild	64	-	-	*			
COV019	81	M	33 (12)	2 (2)	+	DAD / Respiratory failure	Cytomegalovirus infection (adrenal glands)	84	+	-	*			
COV020	81	F	20 (15)	13 (5)	+	DAD / Respiratory failure	Sepsis / Systemic thrombosis	35	+	-	*			
COV021	79	M	20 (13)	15 (7)	+	DAD / Respiratory failure	Sepsis / Sigmoid colon cancer localized	23	+	-	*			
COV022	88	F	21 (9)	11 (7)	+	DAD / Respiratory failure	N/A	86	+	+	*			
COV023	63	M	40 (36)	21 (5)	+	DAD / Respiratory failure	Sepsis / Systemic thrombosis	32	-	-	*			
COV024	54	M	6 (4)	13 (3)	+	DAD / Respiratory failure	Bronchopneumonia severe	27	+	+	*	*		E3
COV025	70	F	35 (29)	11 (7)	+	DAD / Respiratory failure	Bronchopneumonia mild	30	-	-	*			
	Mean 80	M/F 1.5												
Control														
CTL001	75	F				FAR / Circulation failure	N/A	10			*	*	*	C1
CTL002	89	M				AMI / Circulation failure	N/A	22			*	*		C3
CTL003	77	F				Parkinsonism / Respiratory failure	Emaciation / Bronchopneumonia mild	13			*	*	*	C2
CTL004	74	M				ALS / Respiratory failure	Emaciation / Respiratory muscle atrophy	18			*	*		C5
CTL005	70	F				CRC / Cachexia	Emaciation / Bronchopneumonia mild	25			*	*		C4
	Mean 77	M/F 0.7												

F, female; M, male; DAD, diffuse alveolar damage; FAR, fatal arrhythmia; AMI, acute myocadiac infarction; CRC, colorectal cancer; His, histological examination; Mor, morphometrical analysis; Exp, comprehensive mRNA expression analysis; N/A, not applicable; *, Subjected to the examinations; CT severity score was determined on the first CT image from the disease onset according to the criteria proposed by Pan et al., 2020. The two cases were examined postmortem by autopsy imaging (AI). The three were not determined (N/D) because of lack of full lung image. In SARS-Co-V-2 RT-PCR examination with secretory fluid (nasal swab, saliva, or sputum) samples, cases with cycle threshold less than 40 were judged as positive (+). In SARS-Co-V-2 RT-PCR examination with the autopsied lungs, cases with copy number more than 10 per 1 μg were judged as positive (+). In Immunohistochemistry (IHC) for SARS-Co-V2 with the autopsied lungs, cases with more than 3 (degenerated) cells showing unequivocally positive signal were judged as positive (+).

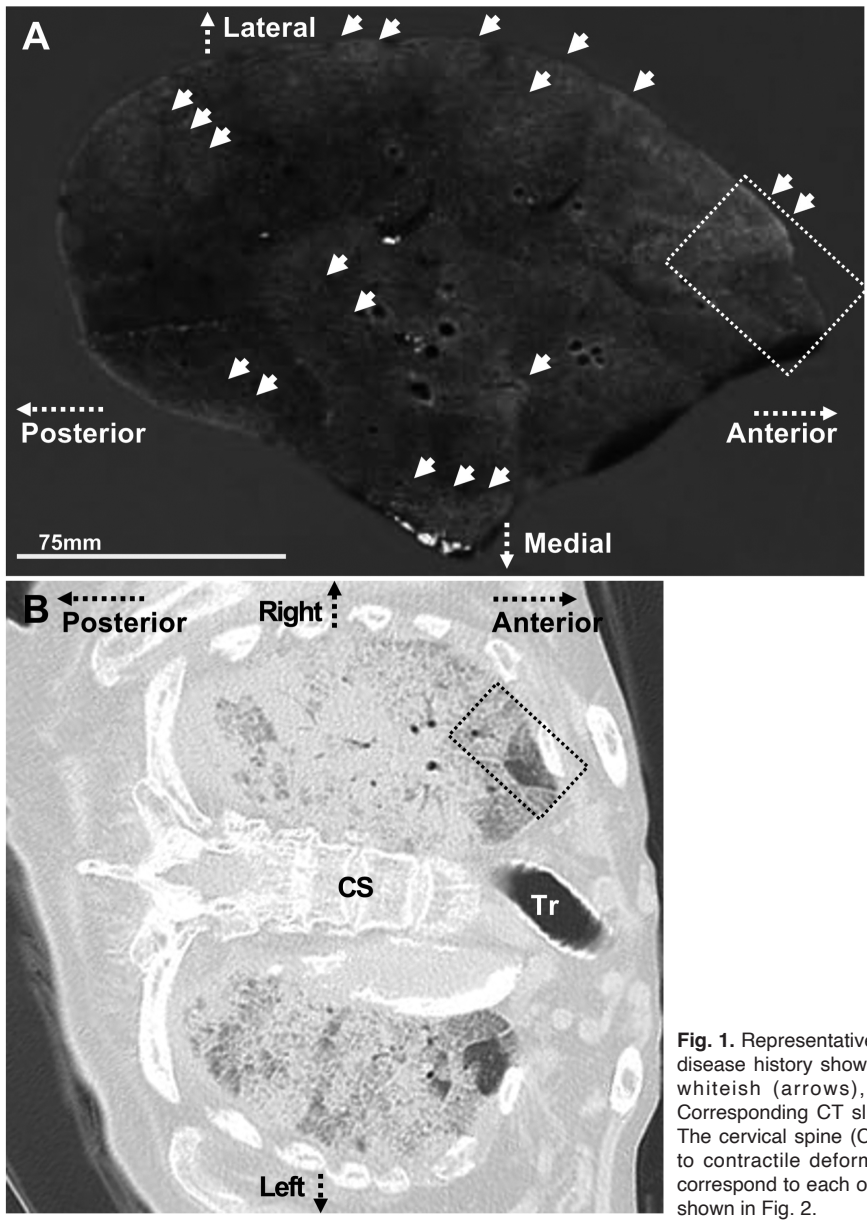

Fig. 1. Representative view of a lung surface cut from a case with a 10-day disease history showing a mosaic pattern. Some areas look slightly gray-whiteish (arrows), whereas the others look almost normal **(A)**. Corresponding CT slice from autopsy imaging examination is shown **(B)**. The cervical spine (CS) and trachea (TR) show abnormal anteflexion due to contractile deformation. The dashed square in the panels A and B correspond to each other. Histological appearance in the dashed square is shown in Fig. 2.

Table 2. Result of KEGG pathway analysis on the upregulated genes in the earliest COVID-19 lesions.

Term	Index	Member (Gene Symbol)	FE	*P* Value
Lysosome	hsa04142	CTSA, ATP6AP1, LAMP1, GLB1, CTSK, GBA, LAPTM5, ARSB, CTSB	7.4	0.00002
Amoebiasis	hsa05146	COL1A1, SERPINB4, LAMA2, COL5A2, PIK3R3, LAMB1, CD14, RAB7A	7.5	0.00008
Glutathione metabolism	hsa00480	GSTM3, G6PD, GPX1, GPX3, ANPEP, GCLM	11.7	0.00013
ECM-receptor interaction	hsa04512	COL1A1, LAMA2, COL5A2, SPP1, TNC, COL6A3, LAMB1	8.0	0.00020
Central carbon metabolism in cancer	hsa05230	G6PD, TIGAR, PKM, PGAM1, PIK3R3	7.8	0.00355
Focal adhesion	hsa04510	COL1A1, LAMA2, COL5A2, SPP1, TNC, PIK3R3, COL6A3, LAMB1	3.9	0.00402
Biosynthesis of amino acids	hsa01230	PKM, PSAT1, PGAM1, TALDO1, BCAT1	6.9	0.00543
PI3K-Akt signaling pathway	hsa04151	COL1A1, LAMA2, COL5A2, DDIT4, SPP1, TNC, PIK3R3, COL6A3, LAMB1	2.6	0.01971
Renin-angiotensin system	hsa04614	CTSA, ANPEP, AGT	13.0	0.02131
Carbon metabolism	hsa01200	G6PD, PKM, PSAT1, PGAM1, TALDO1	4.4	0.02514

FE, Fold Enrichment and P value (Fisher's exact test) were calculated with a public software DAVID.

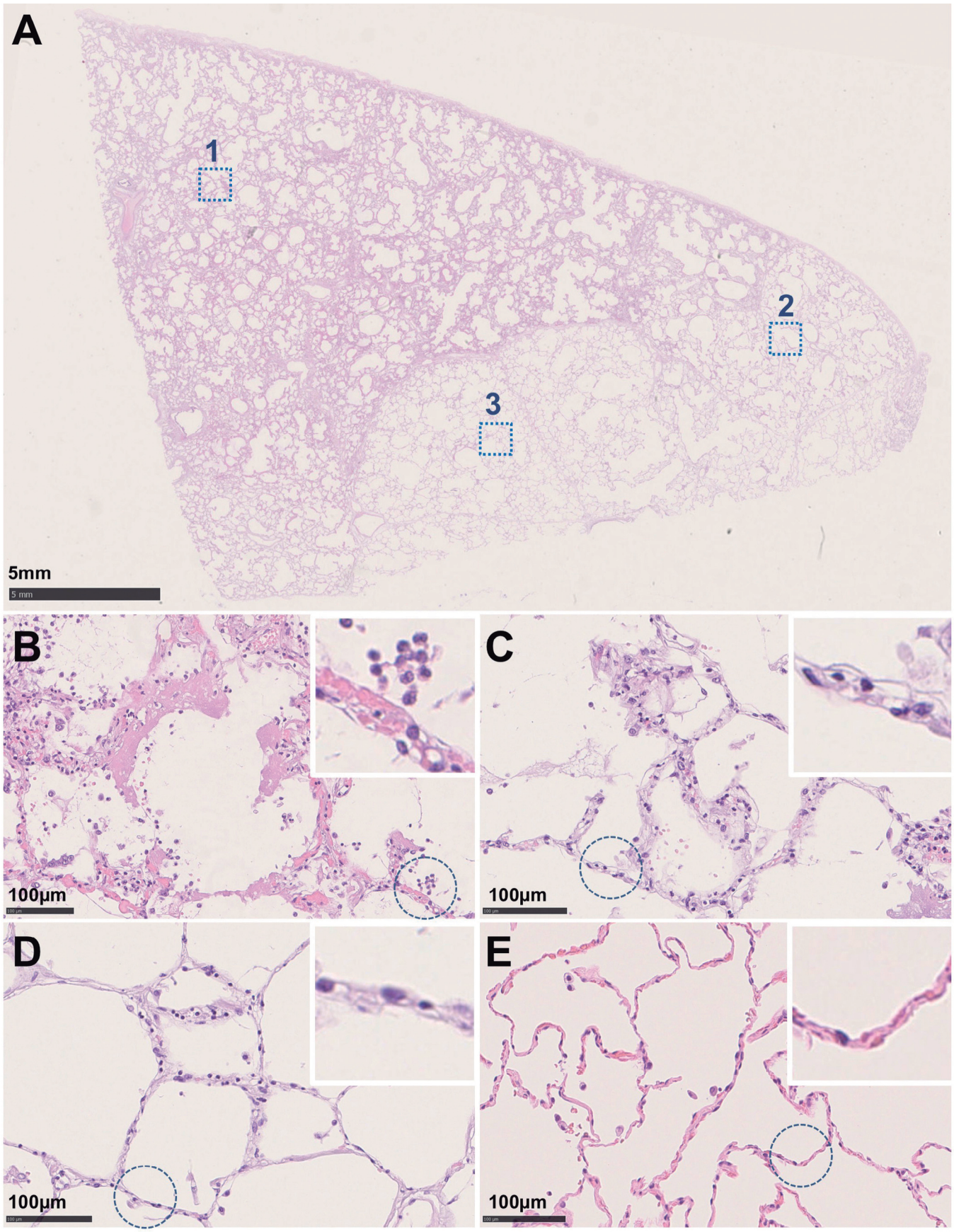

Fig. 2. Representative histopathological photographs from a case with a 10-day disease history. The scanning view panel **A** shows mosaic pattern, that is, there are different temporal phases of alveolar damage observed in each lobule. The dashed squares 1, 2, and 3 are zoomed-in and shown in panels **B, C, and D**, respectively. **B** shows the exudative phase, where thickened alveolar septa with hyaline membranes are observed. **C** shows the earlier exudative phase, where thickened alveolar septa with subtle exudate are observed. **D** shows the putative earliest phase, where capillary dilation and edematous thickening alveolar septa are observed. **E** is the control (autopsy lung from a case with unrelated disease), where no pathological change is observed. The insets are zoom-in views from the dashed circles in each panel.

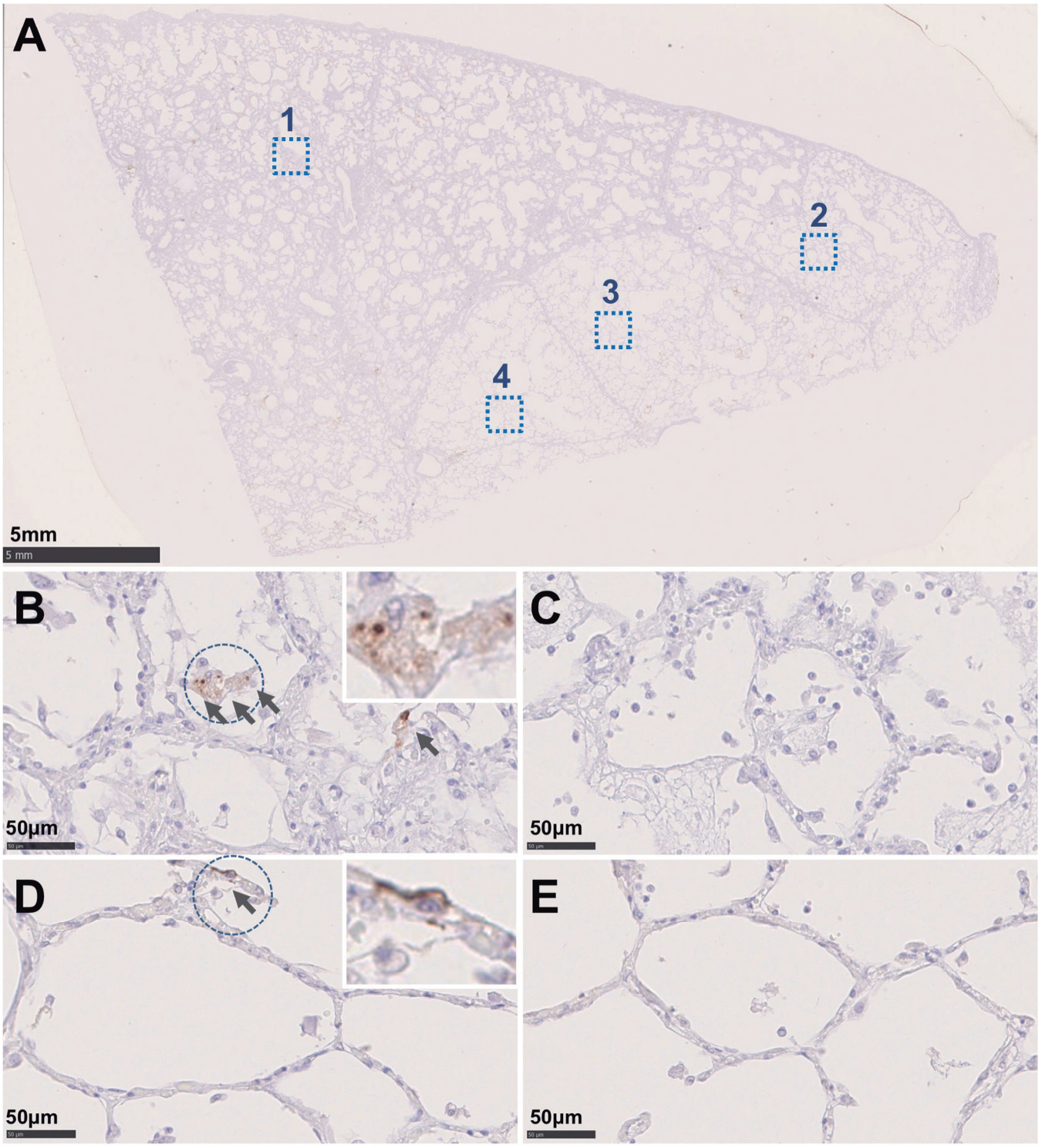

Fig. 3. Immunohistochemical detection of SARS-Co-V2. **A** representative result from a case with a 10-day disease history is shown. The dashed squares 1, 2, and 3 in the scanning view panel A are zoomed-in and shown in the panels **B, C, and D,** respectively. SARS-Co-V2-infected cells are occasionally observed in both the overt exudative lesion (**B**, positive; **C**, negative) and putative earliest lesion (**D**, positive; **E** negative). The insets are zoom-in views from the dashed circles in each panel.

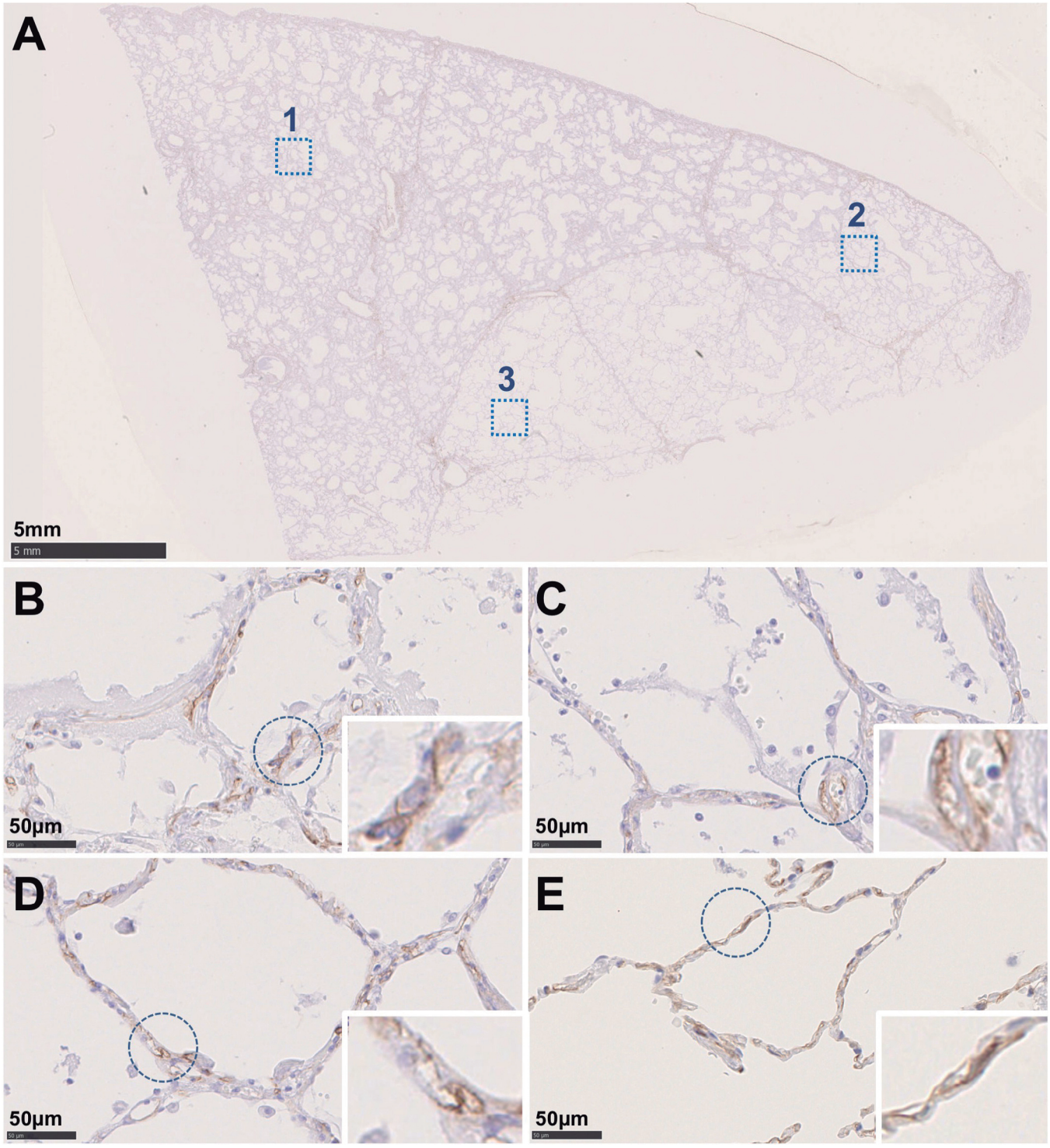

Fig. 4. Immunohistochemical visualization of alveolar capillaries stained with an anti-CD34 antibody. **A** representative result from a case with a 10-day disease history is shown. The dashed squares 1, 2, and 3 in the scanning view panel **A** are zoomed-in and shown in the panels **B, C, and D**, respectively. In the overt exudative lesion **(B)**, alveolar capillaries are discontinuously ruptured. In the earlier exudative lesion **(C)** and putative earliest lesion **(D)**, alveolar capillaries are dilated, compared to the control (**E**, autopsy lung from a case with unrelated disease). The insets are zoom-in views from the dashed circles in each panel.

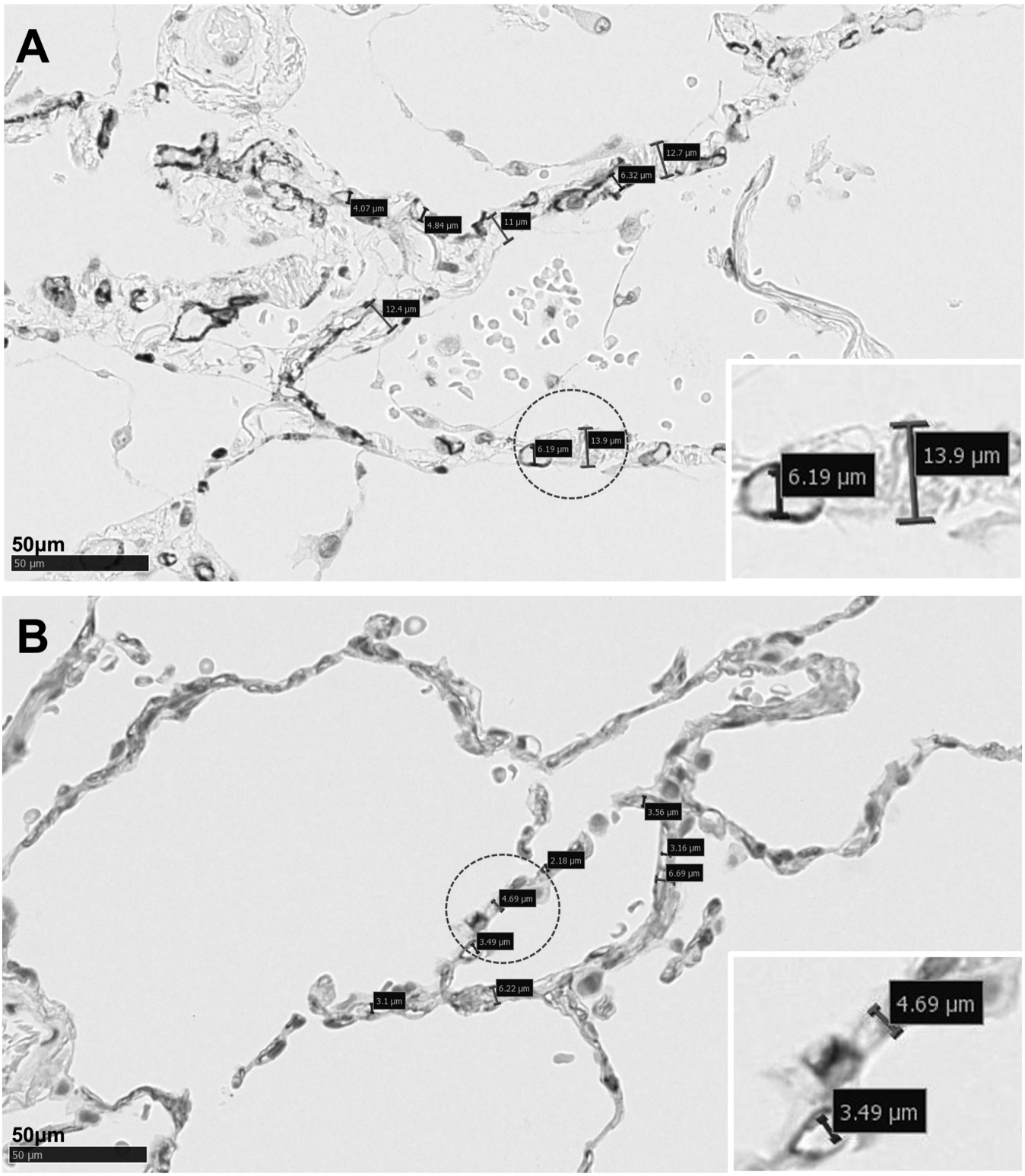

Fig. 5. Representative results of morphometrical analyses. Capillary diameters and alveolar thicknesses in the putative earliest lesion **(A)** and control **(B)** are measured on CD34-immunostained sections. The insets are closed-up views from the dashed circles in each panel.

neutrophils and monocytes, and slight alveolar hemorrhage (Fig. 2A (square 2, 3), 2C, and 2D). These changes agreed well with the earliest putative tissue response in diffuse alveolar damage/acute respiratory distress syndrome (DAD/ARDS) (Thompson et al., 2017). SARS-CoV-2 were immunohistochemically detected in pneumocytes not only in exudative lesions, but also in these earliest lesions (Fig. 3). Thus, we hypothesized that this could be the earliest histopathological change in COVID-19 pneumonia, likely followed by pneumocyte desquamation and hyaline membrane exudation.

Immunohistochemical and morphometrical analyses

To confirm the changes in the alveolar capillaries, we performed immunohistochemistry for a vascular endothelial marker, CD34. To exclude the effect of postmortem congestion, we examined tissue sections from the ventral side of the upper lobe of the lung. The results made the changes clearer, as capillary lumens were found to be dilated (Fig. 4). Morphometric analyses objectively supported the capillary dilation, and also thickening of the alveolar septa (Fig. 5 and Fig. 6).

Immunohistochemistry for the early responders

To further support the significance of the earliest changes, we immunohistochemically examined these lesions for expression of pivotal factors involved in diffuse alveolar damage initiation, such as IL-6, TNF-α, IL-1B, and TF (Bokarewa et al., 2002; Thompson et al., 2017; Leisman et al., 2021; Subrahmanian et al., 2021) (data not shown). Among these, TF was mostly associated with these earliest lesions, where pneumocytes, histocytes/macrophages, and vascular endothelial cells were positive (Fig. 7).

Comprehensive mRNA expression analysis

We also examined these earliest lesions for comprehensive gene expression. Significant changes in expression profiles of these lesions (Fig. 8A) were noted. The KEGG analysis on the upregulated genes whose levels showed 5-fold or more increase in both the two earliest lesions compared to the two controls revealed a remarkable association with the lysosomal pathway (Fig. 8B and Table 2).

Here, we immunohistochemically examined expression of CTSB, one member of the lysosomal pathway, and that confirmed its expression in histocytes/macrophages that were migrating into alveolar interstitium and lumina in these earliest lesions (Fig. 9).

Discussion

Diffuse alveolar damage occurs through a variety of situations, such as acute exacerbation of chronic diffuse interstitial lung disease, terminal stage of malignancies, and severe infectious disease (sepsis) (Thompson et al., 2017). However, discerning the initiating histopathological event in these situations is challenging because of secondary events from multiple factors in a long clinical course, while in COVID-19 pneumonia, spatially and temporally intermittent alveolar damage occurs within relatively short periods (Borczuk, 2021; Bosmuller et al., 2021). Therefore, we consider COVID-19 pneumonia can be a useful material to investigate the initiating event of alveolar damage.

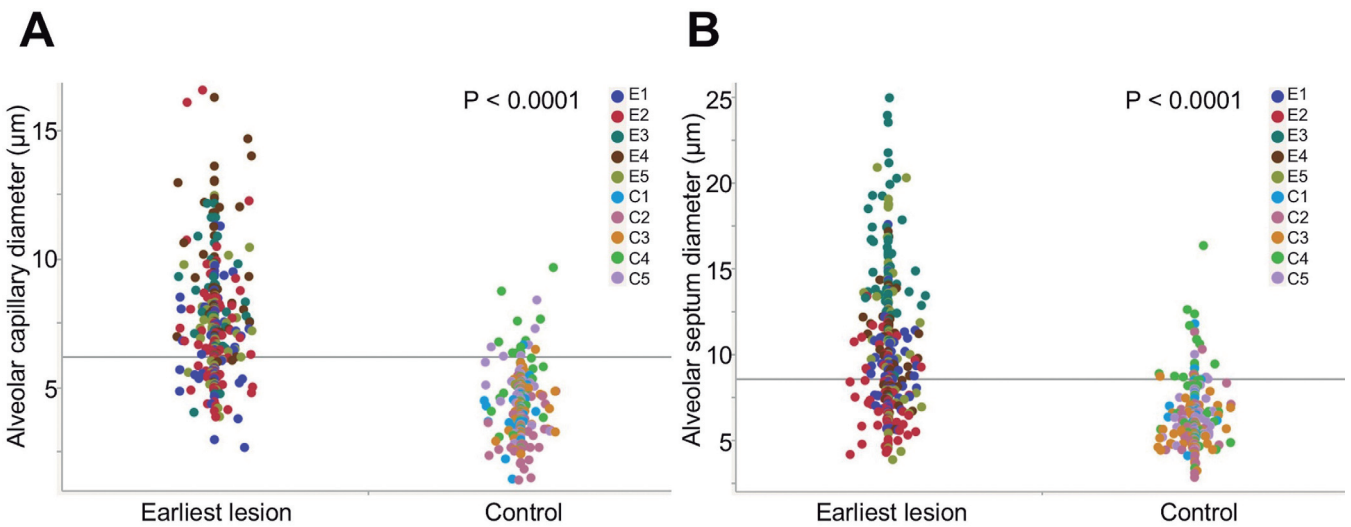

Fig. 6. Capillary diameters and alveolar thicknesses at 50 to 60 points each in putative earliest lesions from five COVID-19 cases (E1-E5) and in normal controls from five autopsy cases of unrelated disease (C1-C5). The values are shown as dot plots. Both capillary diameters and alveolar thicknesses are significantly larger in the earliest lesion. P values calculated with Wilcoxon/Kruskal-Wallis test are shown.

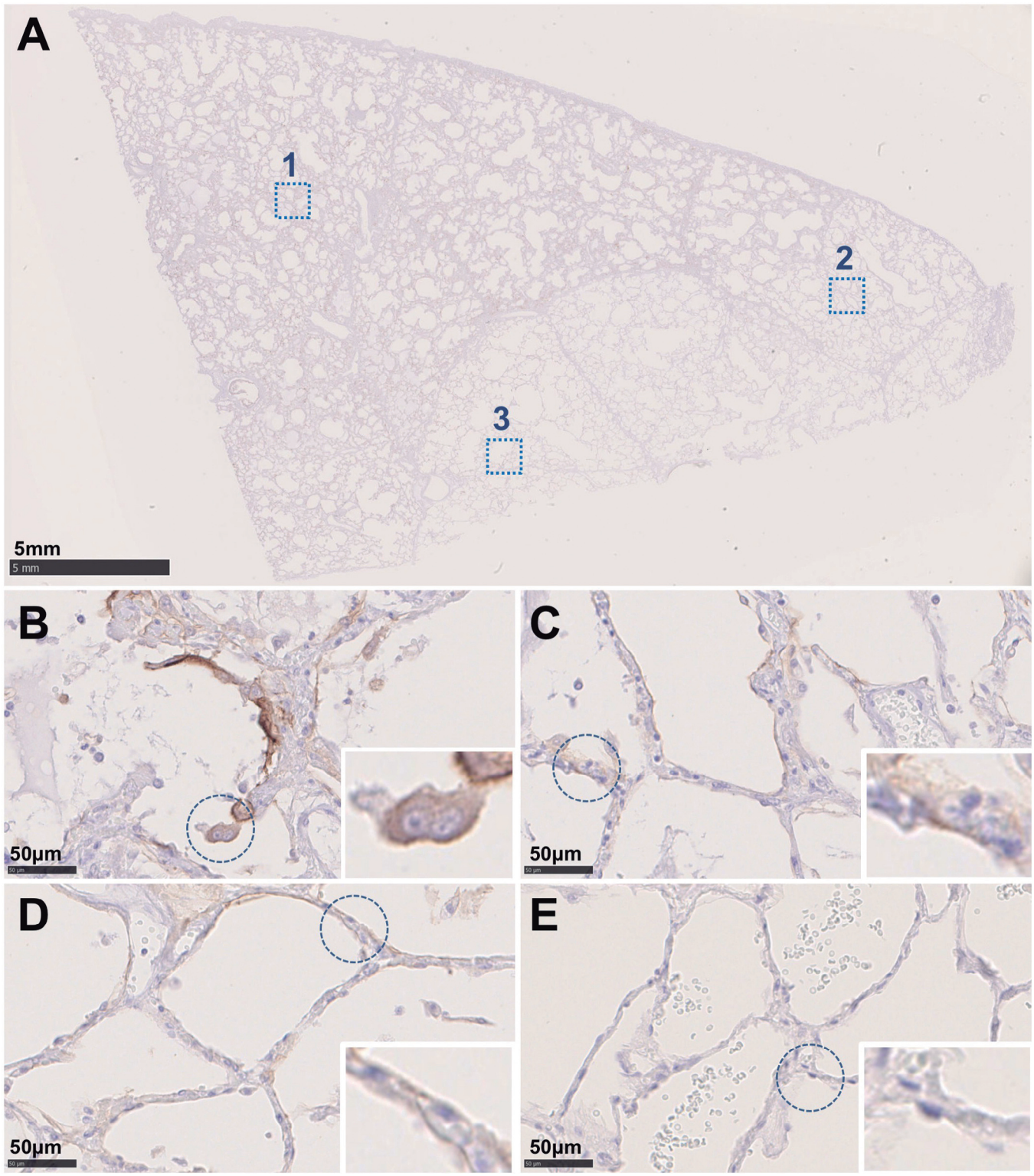

Fig. 7. Immunohistochemical expression of TF. **A** representative result from a case with a 10-day disease history is shown. The dashed squares 1, 2, and 3 in the scanning view panel A are zoomed-in and shown in the panels **B, C, and D**, respectively. In the overt exudative lesion **(B)**, a positive signal is observed in pneumocytes, histocytes/macrophages, endothelial cells, and hyaline membranes. In the earlier exudative lesion **(C)** and putative earliest lesion **(D)**, a positive signal is observed in pneumocytes, histocytes/macrophages, and endothelial cells. In the control (**E**, autopsy lung from a case with unrelated disease), no positive signal is observed. The insets are closed-up views from the dashed circles in each panel.

We examined a series of COVID-19 autopsy cases and particularly focused on temporal histopathological changes. Upon investigating the cases, we found that slight capillary dilation and edematous thickening of the alveolar septa already occurred even in areas that looked almost normal macroscopically, where pneumocytes, histiocytes/macrophages, and endothelial cells were immunohistochemically positive for TF. Thus, we concluded that these could be the earliest detectable changes in histological examinations. Actually, previous studies have reported that focal edema, microscopic alveolar hemorrhage, pneumocyte damage and hyperplasia, macrophage desquamation are earlier changes preceding the exudation (Pernazza et al., 2020; Tian et al., 2020; Bosmuller et al., 2021). Our findings well agree with the previous observations. Also, we would like to mention that such earliest change may be detectable by CT examination, since our autopsy imaging demonstrated that the earliest lesion appeared as very light ground glass opacity. That supports previous reports showing that the CT severity scoring system benefits in prognosis (Chung et al., 2020; Pan et al.,

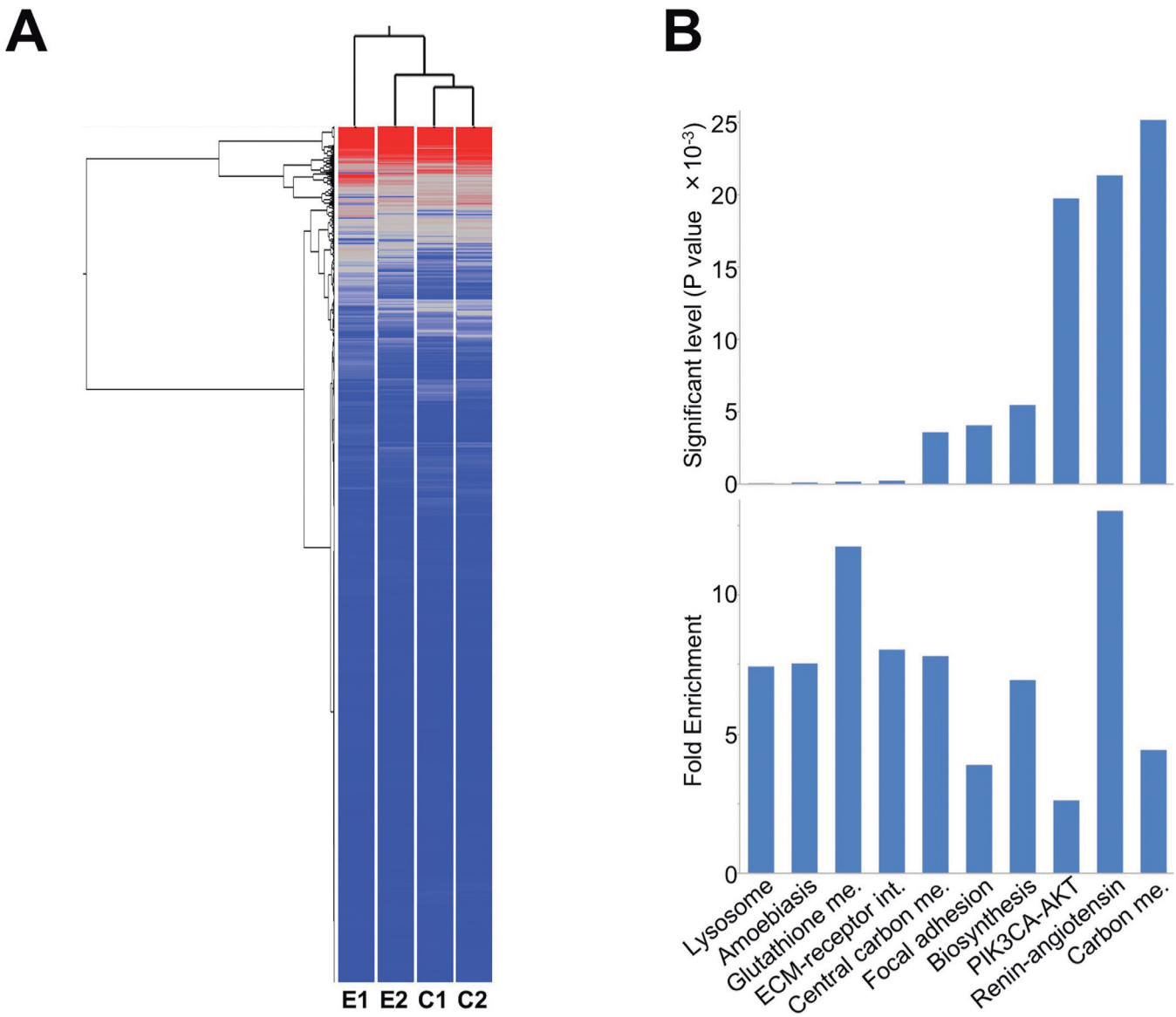

Fig. 8. Comprehensive RNA expression analyses from two earlier lesions (E1 and E2; two different COVID-19 autopsy cases) and two controls (C1 and C2; two different autopsy cases with unrelated disease). A dendrogram is described based on the Ward's hierarchical clustering method **(A)**. E1 and E2 produce distant branches from C1 and C2. The KEGG pathway analysis based on genes whose levels showed 5-fold increase in E1 and E1 compared to C1 and C2 is shown **(B)**. Potentially crucial pathways (horizonal axis) and their significant levels (Fisher's exact test; vertical axis, upper panel) and fold enrichment (vertical axis, lower panel) are presented.

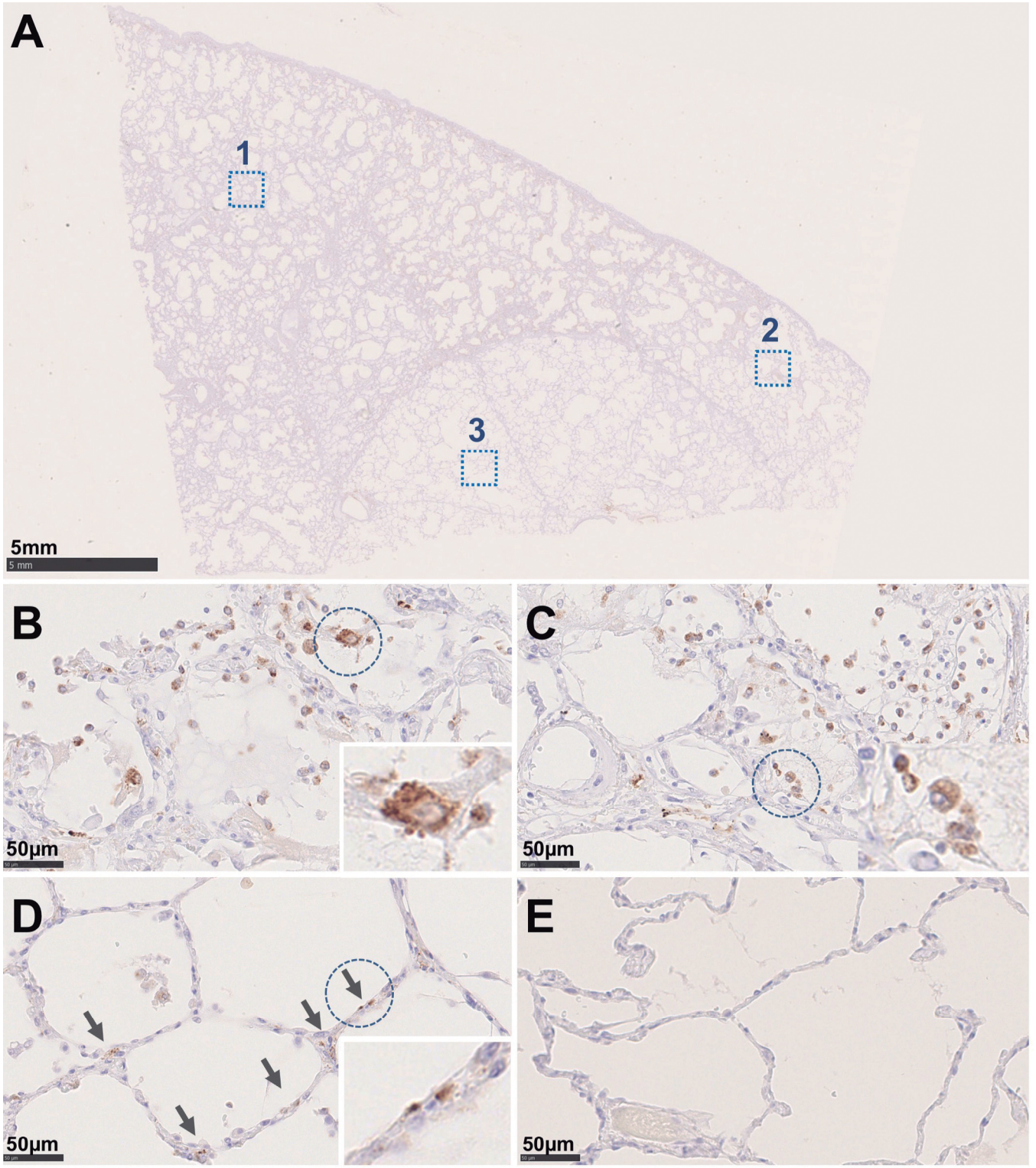

Fig. 9. Immunohistochemical expression of CTSB. **A** representative result from a case with a 10-day disease history is shown. The dashed squares 1, 2, and 3 in the scanning view panel **A** are zoomed-in and shown in the panels **B, C, and D**, respectively. In both the overt **(B)** and earlier **(C)** exudative lesions, numerous histocytes/macrophages with strong positive signal are observed mainly in the alveolar lumina. In the putative earliest lesion **(D),** CTSB-positive histocytes/macrophages are detected mainly in the alveolar interstitium (arrows). In the control (**E**, autopsy lung from a case with unrelated disease), no positive signal is observed although a few resident alveolar macrophages occasionally show a weak signal. The insets are zoom-in views from the dashed circles in each panel.

2020; Brogna et al., 2021).

Here, we investigated gene expression profiles in these earliest lesions and found remarkable upregulation of pathways related to tissue and cell injury, such as lysosome degradation, and extracellular matrix-receptor interaction (Homolak and Kodvanj, 2020; Bugatti, 2021; Lerum et al., 2021; Sorsa et al., 2021; Syed et al., 2021). The finding confirmed the pathological significance of these lesions. Also, it is of great interest to investigate the potential roles of the differentially expressed molecules, as they are assumed to be initiators for alveolar damage. However, on the other hand, the number of samples examined here may not be enough for statistical analyses to draw firm conclusions. There are critical limitations, such as that the total number of autopsy cases is small due to technical difficulty, and that in most cases RNA quality is insufficient due to postmortem degradation. In our series, only two were possible to be subjected to mRNA expression analysis. Thus, accumulation of more autopsy cases with higher RNA quality and further molecular analysis are needed to clear the potential molecular basis in the initiating event of COVID-19 pneumonia.

In summary, we documented that capillary dilation, edematous thickening of alveolar septa could be the earliest histopathological changes in COVID-19 pneumonia. Hopefully, our findings will provide better understanding of not only COVID-19, but also general diffuse alveolar damage.

Acknowledgements. This work was supported by the Smoking Research Foundation (Tokyo, Japan). There are no conflicts of interest.

Contribution of each author was as follows: Okudela-K wrote most parts of the manuscript; Okudela-K, Hayashi-H, Iwashita-H, and Hatayama-Y contributed to the pathological diagnoses. Yoshimura-Y, Sasaki-H, and Miyata-N collected the information of the patients and made clinical data base; Okudela-K performed the morphometrical analyses; Okudela-K, Kataoka-T, and Matsumura-M analyzed the expression profiles; Okudela-K, Tachikawa-N, and Ryo-A designed this study and suggested the content of the manuscript; Mitsui-H carried out the immunohistochemical analyses; Yamashiro-T examined CT images and gave severity scores.

We also thank the technicians at the Division of Pathology of Yokohama City Municipal Hospital for their technical assistance.

References

Bokarewa M.I., Morrissey J.H. and Tarkowski A. (2002). Tissue factor as a proinflammatory agent. Arthritis Res. 4, 190-195.

Borczuk A.C. (2021). Pulmonary pathology of covid-19: A review of autopsy studies. Curr. Opin. Pulm. Med. 27, 184-192.

Bosmuller H., Matter M., Fend F. and Tzankov A. (2021). The pulmonary pathology of covid-19. Virchows Arch. 478, 137-150.

Brogna B., Bignardi E., Brogna C., Volpe M., Lombardi G., Rosa A., Gagliardi G., Capasso P.F.M., Gravino E., Maio F., Pane F., Picariello V., Buono M., Colucci L. and Musto L.A. (2021). A pictorial review of the role of imaging in the detection, management, histopathological correlations, and complications of covid-19 pneumonia. Diagnostics (Basel) 11, 437.

Bugatti K. (2021). αvß6 integrin: An intriguing target for covid-19 and related diseases. Chembiochem 22, 2516-2520.

Chung M., Bernheim A., Mei X., Zhang N., Huang M., Zeng X., Cui J., Xu W., Yang Y., Fayad Z.A., Jacobi A., Li K., Li S. and Shan H. (2020). CT imaging features of 2019 novel coronavirus (2019-ncov). Radiology 295, 202-207.

Homolak J. and Kodvanj I. (2020). Widely available lysosome targeting agents should be considered as potential therapy for COVID-19. Int. J. Antimicrob. Agents 56, 106044.

Hooper J.E., Padera R.F., Dolhnikoff M., da Silva L.F.F., Duarte-Neto A.N., Kapp M.E., Lacy J.M., Mauad T., Saldiva P.H.N., Rapkiewicz A.V., Wolf D.A., Felix J.C., Benson P., Shanes E., Gawelek K.L., Marshall D.A., McDonald M.M., Muller W., Priemer D.S., Solomon I.H., Zak T., Bhattacharjee M.B., Fu L., Gilbert A.R., Harper H.L., Litovsky S., Lomasney J., Mount S.L., Reilly S., Sekulic M., Steffensen T.S., Threlkeld K.J., Zhao B. and Williamson A.K. (2021). A postmortem portrait of the coronavirus disease 2019 (COVID-19) pandemic: A large multi-institutional autopsy survey study. Arch. Pathol. Lab. Med. 145, 529-535.

Leisman D.E., Ronner L., Pinotti R., Taylor M.D., Sinha P., Calfee C.S., Hirayama A.V., Mastroianni F., Turtle C.J., Harhay M.O., Legrand M. and Deutschman C.S. (2021). Assessing the importance of interleukin-6 in covid-19 - authors' reply. Lancet Respir. Med. 9, e14-e15.

Lerum T.V., Maltzahn N.N., Aukrust P., Troseid M., Henriksen K.N., Kasine T., Dyrhol-Riise A.M., Stiksrud B., Haugli M., Blomberg B., Kittang B.R., Johannessen A., Hannula R., Aballi S., Kildal A.B., Eiken R., Dahl T.B., Lund-Johansen F., Muller F., Rodriguez J.R., Meltzer C., Einvik G., Ueland T., Olsen I.C., Consortium N.-S., Barratt-Due A., Aalokken T.M. and Skjonsberg O.H. (2021). Persistent pulmonary pathology after COVID-19 is associated with high viral load, weak antibody response, and high levels of matrix metalloproteinase-9. Sci. Rep. 11, 23205.

Maiese A., Manetti A.C., La Russa R., Di Paolo M., Turillazzi E., Frati P. and Fineschi V. (2021). Autopsy findings in COVID-19-related deaths: A literature review. Forensic Sci. Med. Pathol. 17, 279-296.

Okudela K., Hayashi H., Yoshimura Y., Sasaki H., Horiuchi H., Miyata N., Tachikawa N., Tsuchiya Y., Mitsui H. and Ohashi K. (2020). A japanese case of COVID-19: An autopsy report. Pathol. Int. 70, 820-824.

Pan F., Ye T., Sun P., Gui S., Liang B., Li L., Zheng D., Wang J., Hesketh R.L., Yang L. and Zheng C. (2020). Time course of lung changes at chest ct during recovery from coronavirus disease 2019 (COVID-19). Radiology 295, 715-721.

Pernazza A., Mancini M., Rullo E., Bassi M., De Giacomo T., Rocca C.D. and d'Amati G. (2020). Early histologic findings of pulmonary SARS-CoV-2 infection detected in a surgical specimen. Virchows Arch. 477, 743-748.

Sorsa T., Sahni V., Buduneli N., Gupta S., Raisanen I.T., Golub L.M., Lee H.M., Patila T., Bostanci N., Meurman J., Parnanen P., Nwhator S.O., Singla M. and Gauba K. (2021). Active matrix metalloproteinase-8 (AMMP-8) point-of-care test (POCT) in the COVID-19 pandemic. Expert Rev. Proteomics 18, 707-717.

Subrahmanian S., Borczuk A., Salvatore S., Fung K.M., Merrill J.T., Laurence J. and Ahamed J. (2021). Tissue factor upregulation is associated with SARS-CoV-2 in the lungs of COVID-19 patients. J. Thromb. Haemost. 19, 2268-2274.

Syed F., Li W., Relich R.F., Russell P.M., Zhang S., Zimmerman M.K. and Yu Q. (2021). Excessive matrix metalloproteinase-1 and hyperactivation of endothelial cells occurred in COVID-19 patients and were associated with the severity of covid-19. J. Infect. Dis. 224, 60-69.

Thompson B.T., Chambers R.C. and Liu K.D. (2017). Acute respiratory distress syndrome. N. Engl. J. Med. 377, 1904-1905.

Tian S., Hu W., Niu L., Liu H., Xu H. and Xiao S.Y. (2020). Pulmonary pathology of early-phase 2019 novel coronavirus (COVID-19) pneumonia in two patients with lung cancer. J. Thorac. Oncol. 15, 700-704.

Yamaoka Y., Miyakawa K., Jeremiah S.S., Funabashi R., Okudela K., Kikuchi S., Katada J., Wada A., Takei T., Nishi M., Shimizu K., Ozawa H., Usuku S., Kawakami C., Tanaka N., Morita T., Hayashi H., Mitsui H., Suzuki K., Aizawa D., Yoshimura Y., Miyazaki T., Yamazaki E., Suzuki T., Kimura H., Shimizu H., Okabe N., Hasegawa H. and Ryo A. (2021). Highly specific monoclonal antibodies and epitope identification against SARS-CoV-2 nucleocapsid protein for antigen detection tests. Cell Rep. Med. 2, 100311.

Accepted December 1, 2022